Andrzej ŁASICA, Konrad SOBOLEWSKI, Jacek STARZYŃSKI

DOI: 10.15199/48.2025.04.17

Design of compact high-speed Marx generator

Projekt kompaktowego generatora Marxa przebiegów nanosekundowych

Abstract. *The article is devoted to the design of a compact nanosecond pulse generator, based on Marx's idea. Computer simulation was used in the design process. Based on the results obtained in this way, the design of the prototype was optimised so that the amplitude of the generated pulses was as large as possible. As a result of the design work, an 11-stage surge generator was made with an output pulse rise time of about 20 ns and an amplitude of about 200 kV.*

Streszczenie. *Artykuł poświęcony jest projektowaniu kompaktowego generatora impulsów nanosekundowych, opartego na układzie Marxa. W procesie projektowania wykorzystano symulacje komputerowe. Na podstawie uzyskanych w ten sposób wyników zoptymalizowano projekt urządzenia tak, aby amplituda generowanych impulsów była jak największa. W wyniku prac projektowych wykonano 11-stopniowy generator udarowy o czasie narastania impulsu wyjściowego około 20 ns i amplitudzie około 200 kV.*

Keywords: HV pulses; Marx generator; compact HV generator; high-speed generator; electromagnetic compatibility; electromagnetic immunity testing
Słowa kluczowe: impulsy wysokonapięciowe, generator Marxa, kompaktowy generator wysokiego napięcia, generator impulsowy, kompatybilność elektromagnetyczna, badanie odporności

Introduction

Despite their long history, generators developed based on the idea presented by Erwin Otto Marx [1] are still the most popular devices for producing high-voltage pulses with rise times of micro and nanoseconds. Their task is to generate a high-voltage pulse using a low-voltage DC source. Marx generators are used in high-energy physics experiments to simulate lightning discharges' effects on power lines and network equipment. In addition to typical microsecond shapes and voltage surges for performing immunity tests on power equipment following the standard EN 60060-1 [2], there are applications of much faster nanosecond pulses. These may, for example, mimic NEMP [3, 4] or HEMP [5] when testing civil or military equipment, similar to MIL-STD-461G [6, 7]. In addition to the commercial generators for standardized pulses, e.g., [8, 9, 10], laboratory generators are being built for non-typical, eventually stronger pulses [11, 12, 13, 14].

The paper is focused on the presentation of computer validation, verification and optimisation of compact, high-speed Marx generators. The generator diagram is quite classical, yet its geometry is optimised to reduce the parasitic inductance and thus to get the possibly fast pulses and high efficiency. Erwin Otto Marx proposed the classical structure of the pulse generator in 1924 [15]. It aimed to generate a high-voltage pulse from a low-voltage DC supply. The electrical scheme of the generator is shown in Fig. 1.

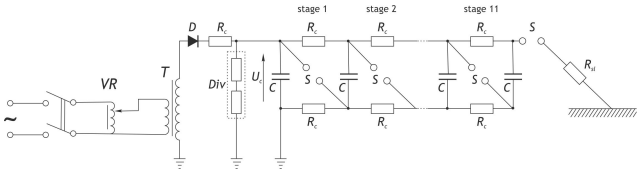

Fig. 1. The classical structure of the Marx generator connected to a 100 Ω load. VR – voltage regulator, T – transformer, D – diode, R_c – loading resistors, S – spark gaps, C – capacitors, R_{sl} – load resistor, U_c – charging voltage.

Marx's idea was based on electrically charging N identical capacitors in parallel connection and then reconnecting them to a series to get input voltage multiplied N times. For that purpose, a structure of resistors and spark gaps is used, where resistors limit the charging current and provide an interstage impedance barrier to direct the discharge current through the load. The basic idea can easily be understood and described with an analytical formula, which was done in this paper's next part. However, using more elaborate and realistic computer models allows designers to build more sophisticated structures of higher performance.

Analytical approach

The presented design aims to obtain a structure that is as compact as possible, delivering voltage pulses of as high as possible magnitude, a shape of T_p=50 ns wide, and a rise time of a few nanoseconds. The method of determining the time parameters of stroke is presented in Fig. 2.

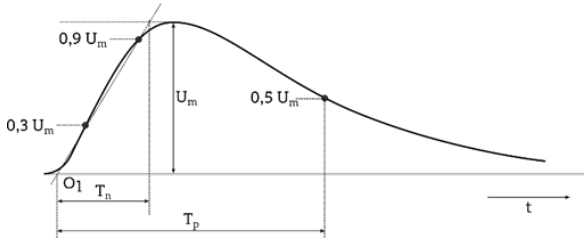

Fig. 2. Method of determining the time parameters of the pulse.

The basic parameters of such a design can be obtained with a simplified analytical formula [16]. The effective capacitance of the firing generator equals C/N, where optimised C – capacitance, N - number of capacitors. It is discharged through the load R_L and parasitic (internal) impedance created by the device structure and connecting cables. The internal impedance can be considered a combination of resistance (built by arc resistances of the spark gaps) and parasitic inductance of capacitors and connections. Neglecting the internal impedance makes it possible to estimate the total duration of the output pulse as Eq. 1:

$$T_p \approx 5\frac{C}{N}R_L. \tag{1}$$

Furthermore, describe the discharging pulse with the Eq. 2:

$$U_p(t) = NU_c e^{-\frac{tN}{CR_L}}. \tag{2}$$

The generator model was significantly simplified for this estimation by neglecting common capacitances and inductances. However, even then, we can predict the number and parameters of capacitors needed to build the generator. Assuming that the presented model was equipped with suppliers, it will provide $U_s = 50\ kV$ output and predicted $N = 11$ stages of the generator, allowing it to reach the desired $U_{pmax} = 500\ kV$ at the output. Using the Eq. 2 and assuming $T_p = 50\ ns$ pulse width (at this time, the voltage should drop to half of the magnitude), we shall get:

(3) $$0.5 = e^{-\frac{11 \cdot 5 \cdot 10^{-8}}{100 \cdot C}},$$

giving:

(4) $$C = -\frac{11 \cdot 5 \cdot 10^{-8}}{100 \cdot \ln(0.5)} = 7.9348 \cdot 10^{-9} \approx 8 \text{ [nF]}.$$

The pulse's rise time is determined mainly by the parasitic inductance of the generator. An initial assumption about the generator geometry needs to be made to estimate this parameter. The presented design assumed capacitors should be placed in one row, and spark gaps should be installed between them, as shown in Fig. 3.

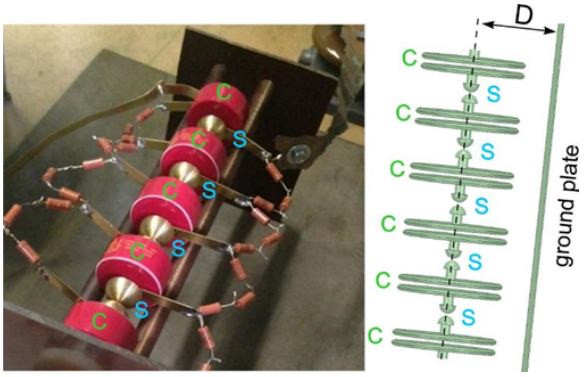

Fig. 3. The basic idea of constructing a row of capacitors with spark gaps between them: the left inset shows a view of the prototype generator, and the right one presents the geometry of the metal parts: capacitor plates, connections and spark gap electrode.

Such construction minimises the total length of connections in the firing generator, and thus, it should also reduce the parasitic inductance. The most simplified model of a firing generator can be imagined as a long cylindrical rod of varying diameter placed above a metal strip – a return conductor. The analytical formula for the equivalent unit (per 1 meter of length) inductance of two parallel conductors, which can be found in any electromagnetic textbook, reads:

(5) $$L_u \approx \frac{\mu}{\pi} \ln(\frac{D}{r_g}) \text{ [H/m]},$$

where: $\mu = \mu_r \mu_0$ is the magnetic permeability of the medium (model assumed $\mu_r = 1$), D is the distance between the conductors, and r_g is their mean geometrical radius.

As can be seen, the smaller the r_g is, the higher inductance we shall get. In our case, the absolute radius of the capacitors connected in series varies from the plate radius (about 50 mm) to the radius of the spark within the gaps. Assuming the computationally worst case (smallest value equal to the spark radius) $r_g = 1\ mm$, then assuming a $D = 150\ mm$ distance between the row of spark gaps and the return conductor, allows us to estimate the value of $L_u = 2\ \mu H/m$.

Next, it has been assumed that the total length of the generator can reach $l_g = 1m$, and taking into account the load resistance, that can estimate the time constant of the output pulse for $L/R_{sl} \approx 2000/100 = 10\ ns$. It is, of course, just a rough estimate, but the value seems satisfactory at this design stage. It should be remembered that the speed and synchronisation of the spark gaps will significantly affect the pulse's rising slope.

The last design parameters that needed to be estimated were the values of charging resistors. As was already mentioned, they play two crucial roles. The first one is limiting the charging current, which allows matching the generator to the actual supply capabilities. For many applications, getting a device offering a high repetition rate would be advantageous, as would applying a short series of pulses if necessary. However, high repetition requires fast charging of capacitors, which strains both the supply system and capacitors. Therefore, a relatively high resistance value should be selected, allowing for slow charging with a not-so-high current.

The presented generator shall charge N=11 capacitors $C = 8\ nF$, connected in parallel, giving an equivalent capacitance of $C_{equiv} = 88\ nF$ (for further analysis, it has been assumed $C_{equiv} = 90\ nF$). Considering the time constant of the RC circuit, it was calculated that for a repetition rate of $R_R = 3$ pulses per second. This way, capacitors should be charged in 300 ms, which limits the time constant $\tau = RC$ to $\tau = 0.06\ s$, and, for given $C_{equiv} = 90\ nF$, they need $R_c = 666\ k\Omega$ charging resistance. An $i_c = 75\ mA$ peak current power supply was required for such charging.

Lumped numerical model

A numerical model of the generator was implemented in the ANSYS Simplorer environment to verify the predictions obtained in the previous section. ANSYS Simplorer is an advanced and multidisciplinary circuit simulator that analyses all aspects of large-scale systems, from detailed component analysis to system performance, in one virtual design environment. The program has an extensive library of elements, including electric, magnetic, mechanical, hydraulic, control elements, SMPS-extending, models of batteries, and PFC filters and converters. It also has an easy-to-use interface and is characterised by a high speed of operation. The edited screenshot with the view of the model is presented in Fig. 4.

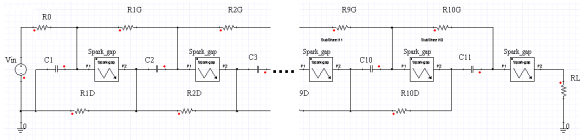

Fig. 4. The edited view of the ANSYS Simplorer generator model: the middle sections have been removed to change the picture proportions to make it readable.

The model has been created using the standard elements from the Simplorer library, like resistors and capacitors. An additional element, a good realistic model of the spark gap, was implemented based on the Basso model [17, 18] – see Fig. 5. This model has been chosen as optimal for solving this task. However, more complicated models exist in the literature, like the Pouncey-Lehr model, also used to simulate spark gap element and arc phenomena [19]. However, this model is much more complicated, and its structure considers parameters that are not essential to this simulation.

Spark gaps are highly nonlinear devices used repetitively in ignition-type circuits. The typical spark gap is made by two electrodes facing each other across a short distance, which a dielectric material fulfils. The gap between electrodes, in this case, is filled with air. If the voltage applied to the electrodes is below its striking voltage, the current flowing through the spark gap is close to zero. Once the striking voltage is attained, the voltage across the spark gap suddenly collapses to the glow voltage value. If the current still increases, the voltage decreases further to the arc voltage level. The spark gap stays conductive until its current falls

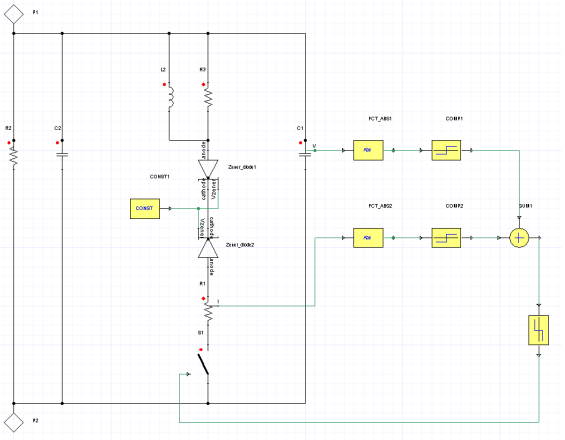

Fig. 5. Simplorer model of the spark gap according to [14]: two Zener diodes (Zener diode 1, Zener diode 2) represent arc voltage, and the switch (S1) is closed by a threshold value of the voltage (FCT_ABS1) or sustaining threshold current (FCT_ABS2); both value.

below a sustaining value, like a thyristor.

Figure 6 shows exemplary time plots of the voltages observed on the first (C_1) and the last (C_{11}) capacitors and the output pulses of the generator. A comparison of the simulation results with the waveforms measured in the prototype is presented in Section 6 of this article. The charging voltage was set to values for these simulations depending on future laboratory test possibilities. The spark gap voltage threshold was set to values that determined the pulse repetition time close to $t_t = 300\ ms$. The first charging resistor of $R_{CH} = 666\ k\Omega$ was taken, and all inter-stage resistances were set to $R_{C1} = 2.5\ k\Omega$, $R_{C2} = 6\ k\Omega$ or $R_{C3} = 450\ k\Omega$ depending on the laboratory test setup taken in the next step of research.

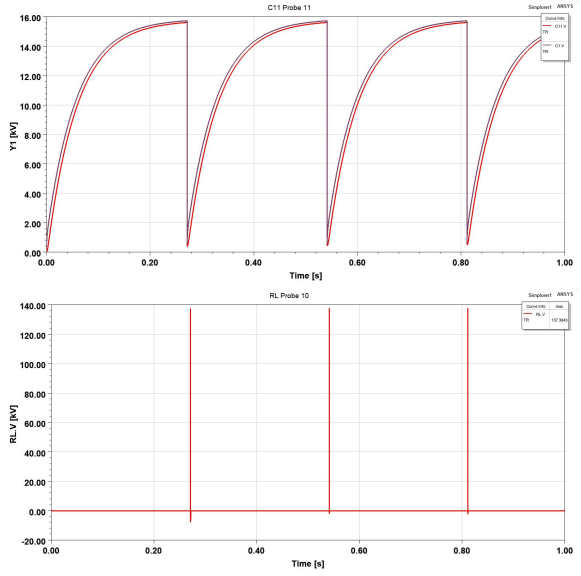

Fig. 6. Exemplary simulation results of 11-stage Marx generator: charging voltages of the first and the last capacitors (upper inset) and the output pulses - lower plot.

The single pulse, shown in detail in Fig. 7, is compatible with predictions (estimates according to Eq. 1 and Eq. 2): its magnitude reaches over 130 kV. Its width (to the half of magnitude) is about 75 ns. The differences are caused by a much more realistic model, taking into account additional (to the load) impedance discharging the capacitors. The length of the pulse front can be estimated at 10-11 ns, but it should

Table 1. Variant designs of generators compared

$R_{ch}\ [k\Omega]$	$U_c\ [kV]$	$\lvert U_p\rvert\ [kV]$	$E_U\ [\%]$
2.5	52	421.71	73.7
6	17	153.18	81.91
6	20	180.80	82.18
450	15	81.21	49.2
450	20	108.90	49.5

be mentioned that this value is strongly affected by the spark gap model parameters.

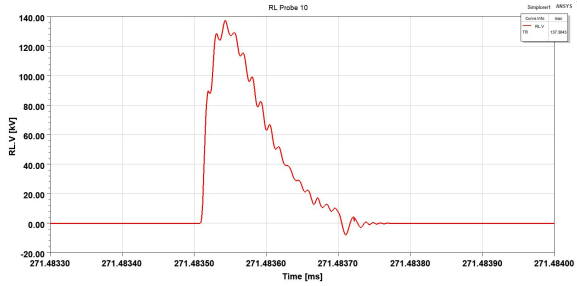

Fig. 7. Exemplary simulation result of 11-stage Marx generator: A single pulse in a stretched time base.

The numerical model builds a convenient platform for analysing different design variants. In this case, it made it possible to quickly check the influence of the deviations of element values, calculate the power efficiency of the generator, and simulate different faults of selected elements. Exemplary results for interstage resistor selection are presented below. They contain simulated five designs with interstage resistors equal to R_{C1}=2.5 kΩ, $R_{C2} = 6\ k\Omega$ or $R_{C3} = 450\ k\Omega$ as used in further research. The voltage efficiency of the generator can be calculated with the Eq. 6:

$$e_U = \frac{U_p}{N \cdot U_c} 100\%, \tag{6}$$

where: e_U - generator voltage efficiency, U_P - maximum output voltage, U_C - charging voltage, N - number of stages.

Table 1 presents selected parameters: the value of interstage resistors, the magnitude of charging voltage, the magnitude of the output pulse and maximal voltage efficiency for the five variants of generator design mentioned above. It can be seen that as long as the interstage resistors are much smaller than the charging one and much bigger than the load, their value does not significantly affect the characteristics of the generator.

Prototype

As described in previous sections of this paper, the design aims to build a compact structure delivering pulses of as high as possible magnitude, 50 nanoseconds wide and a rise time of a few nanoseconds. A view of the 11-stage generator built based on the presented simulation analysis and assumptions is shown in Fig. 8.

As mentioned earlier, 11 ceramic capacitors with a capacity of $C = 8\ nF$ and a voltage of $U_c = 50\ kV$ have been used for construction. In the first version, non-inductive carbon resistors with a resistance of $R_C = 450\ k\Omega$ each were used as charging resistors (both on the HV side and the ground side). The whole construction was placed in a hermetic tube that inflates it. Paschen's law also allows regulating the ignition voltage of the spark gaps without changing their spacing by variable pressure settings [20]. The second version of the generator uses $R_C = 6\ k\Omega$ interstage resis-

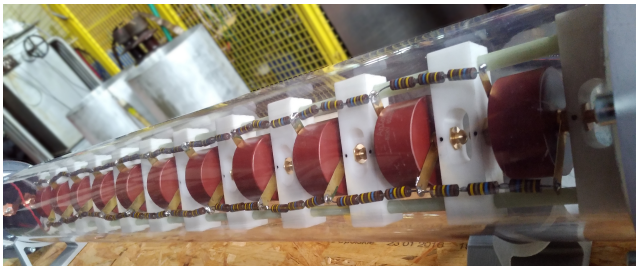

Fig. 8. 11-stage Marx generator.

tors. The generator was powered by a DC-DC converter, the design of which is described in detail in [21].

Practical tests

Measuring output voltages with amplitudes of hundreds of kilovolts and rise times of single nanoseconds using voltage dividers is technically very difficult to do. Therefore, it was decided to make an indirect measurement using the measurement of the electric field. A stripline with an impedance of $Z_s = 130\ \Omega$ was connected to the generator output during the tests. The height of the line was $h_s = 30\ cm$. Taking advantage of the fact that the field strength is uniform under the stripline, the field strength measured values were converted into the value of the output voltage.

The electric field was measured with the Montena D-dot SGE3-5G probe [22]. The waveform was observed and scaled on a Lecroy 640Zi oscilloscope. The measuring probe was connected to the oscilloscope by a Montena MOL3000 fibre optic link [23]. The high-speed sampling rate was a significant parameter of using devices and a very high-frequency measurement range. The scheme of the measuring system is shown in Fig. 9.

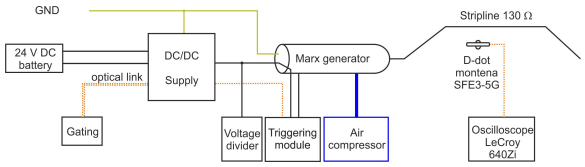

Fig. 9. Measuring system diagram.

Four series of measurements have been made. The first two were done for $R_C = 450\ k\Omega$ interstage resistors, and the next for $R_C = 6\ k\Omega$ interstage resistors. Series 1 and 3 were made at atmospheric pressure in the generator tube. These assumptions allowed the stable operation of the generator at $U_c = 15\ kV$ charging voltage. Series 2 and 4 were made at 2 atmospheres of overpressure. In this case, the generator charging voltage might be raised to $U_c = 20\ kV$. Sample waveforms obtained for each measurement series are shown in Fig. 10a - Fig. 10d.

The summarisation of measurement results is shown in Table 2. Labeling the columns are as follows: R_C - the value of interstage resistors, U_C - charging voltage, Emax - peak value of electric field pulse, e_{ff} - generator efficiency calculated from the Eq. 7:

$$e_{ff} = \frac{E_{max} h}{N U_c}, \tag{7}$$

where: E_{max} - peak value of the electric field, h - the height of the stripline ($h = 0.3\ m$), N - number of generator stages ($N = 11$), U_C - charging voltage.

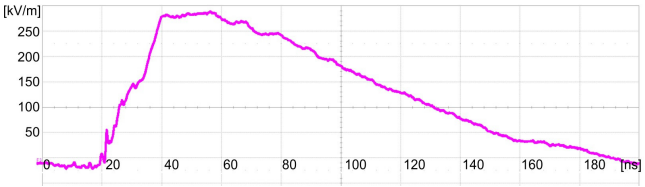

(a) $R_C = 450\ k\Omega$ interstage resistors and $U_C = 15\ kV$ charging voltage; 50 (kV/m)/div; Timebase 20 ns/div.

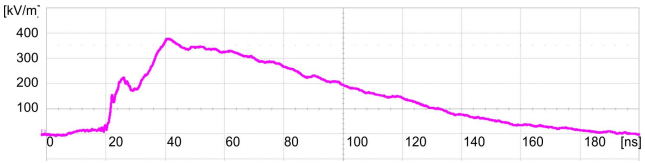

(b) $R_C = 450\ k\Omega$ interstage resistors and $U_C = 20\ kV$ charging voltage; 100 (kV/m)/div; Timebase 20 ns/div.

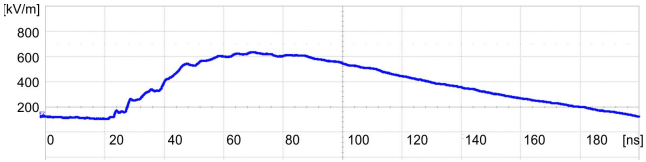

(c) $R_C = 6\ k\Omega$ interstage resistors and $U_C = 17\ kV$ charging voltage; 200 (kV/m)/div; Timebase 20 ns/div.

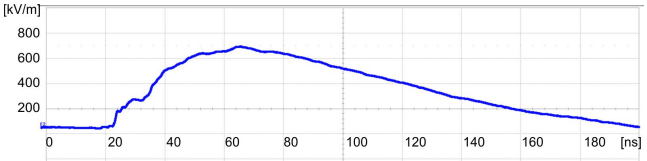

(d) $R_C = 6\ k\Omega$ interstage resistors and $U_C = 20\ kV$ charging voltage; 200 (kV/m)/div; Timebase 20 ns/div.

Fig. 10. Exemplary results of the electric field inside stripline connected to the output of 11-stage Marx generator with various resistor R_C and voltages U_C values.

Table 2. Summarisation of measurement results.

$R_c\ [k\Omega]$	$U_c\ [kV]$	$U_{load}\ [kV]$	$E_{max}\ [kV/m]$	$e_{ff}\ [\%]$
6	17	153.3	511	82.0
6	20	192.0	640	87.3
450	15	89.7	299	54.4
450	20	113.7	379	51.7

Conclusions

The presented paper describes the procedure of designing a high-speed Marx generator with parallel verification of actual measurements and computer simulations. The results obtained in the performed circuit model with the results of the prototype examination have been compared in Fig. 11a - Fig. 11d.

The research results confirmed that it is possible to make a high-speed Marx generator model that complies with its simulation prototype.

Comparing the results of the numerical model and the prototype (Table 3 and Fig. 11a - Fig. 11d) confirmed the model's compliance. This experiment gives new possibilities for prototyping this type of generator. The first surprising relationship obtained using the model was showing that the value of interstage charging resistors impacts the gener-

Table 3. Summarisation of measurement results.

$R_c\ [k\Omega]$	$U_c\ [kV]$	$e_{U\ simulation}\ [\%]$	$e_{ff\ prototype}\ [\%]$
6	17	81.9	82.0
6	20	82.2	87.3
450	15	49.2	54.4
450	20	49.5	51.7

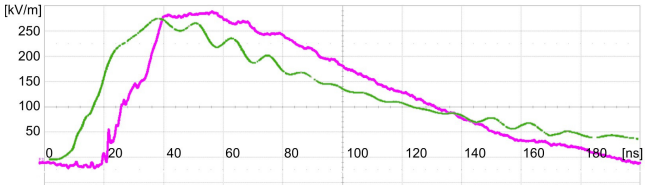

(a) $R_C = 450\ k\Omega$ interstage resistors and $U_C = 15\ kV$ charging voltage (magenta) and the electric field determined by the simulation (green); 50 (kV/m)/div; Timebase 20 ns/div.

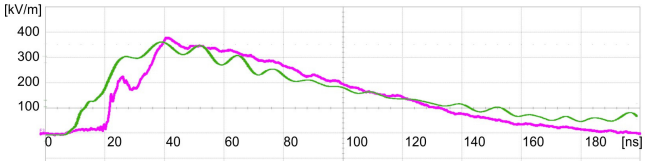

(b) $R_C = 450\ k\Omega$ interstage resistors and $U_C = 20\ kV$ charging voltage (magenta) and the electric field determined by the simulation (green); 100 (kV/m)/div; Timebase 20 ns/div.

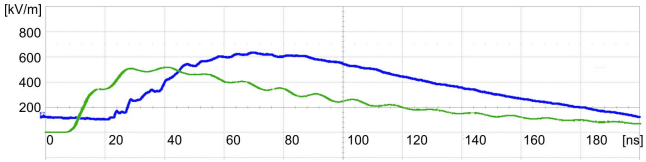

(c) $R_C = 6\ k\Omega$ interstage resistors and $U_C = 17\ kV$ charging voltage (blue) and the electric field determined by the simulation (green); 200 (kV/m)/div; Timebase 20 ns/div.

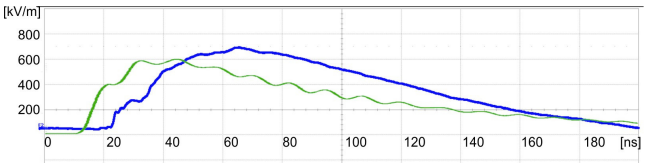

(d) $R_C = 6\ k\Omega$ interstage resistors and $U_C = 20\ kV$ charging volt-age (blue) and the electric field determined by the simulation (green); 200 (kV/m)/div; Timebase 20 ns/div.

Fig. 11. Comparison of the electric field in the stripline generated from the 11-stage Marx generator with various resistor R_C and voltages U_C values.

ator's voltage efficiency. Of course, the lower value of these resistances leads to a greater frequency of repetition of the generated impulses and a higher amplitude of the generated surges. Finally, the voltage efficiency of the device is more remarkable.

Authors: *Ph.D. Andrzej Łasica, Ph.D. Konrad Sobolewski, Prof. Jacek Starzyński, Institute of Theory of Electrical Engineering, Measurement and Information Systems, Facultyof Electrical Engineering, Warsaw University of Technology,ul. Koszykowa 75, 00-662 Warszawa, Poland, email: andrzej.lasica@pw.edu.pl*

REFERENCES

[1] Marx E., Versuche über die Prüfung von Isolatoren mit Spanningsstößen [Experiments on the Testing of Insulators using High Voltage Pulses], Elektrotechnische Zeitschrift, ISSN 0424-0200, 1925.
[2] PN-EN 60060-1: 2011, High-voltage test techniques - Part 1: General definitions and test requirements.
[3] Raju M., Sarma V., Satav S., Rao K., Narayana K., Sholapurwala Z.: Fast Transient High Voltage Pulse Radiating System for vulnerability studies of NEMP on Electronic systems, 10th International Conference on Electromagnetic Interference Compatibility, pp. 223–228, 2008.
[4] Jung M., Weise T., Nitsch D., Braunsberger U.: Upgrade of a 350 kV NEMP HPD pulser to 1.2 MV, Conference Record of the Twenty-Sixth International Power Modulator Symposium, pp. 356–359, 2004, [doi] 10.1109/MODSYM.2004.1433585.
[5] Jiang H.: Design of a Marx Generator for HEMP filter evaluation taking account of parasitic effect of components, 2016 International Symposium on Electromagnetic Compatibility - EMC EUROPE, pp. 839–843, 2016, [doi] 10.1109/EMCEurope.2016.7739191.
[6] PMIL-STD-461G, Requirements for the Control of Electromagnetic Interference Characteristics of Subsystems and Equipment.
[7] Sabath F., Potthast S.: Wartości tolerancji i poziom ufności dla testów terenowych impulsów elektromagnetycznych na dużych wysokościach (HEMP), IEEE Transactions on Electromagnetic Compatibility, 2016, [doi] doi.org/10.1109/TEMC.2012.2237032.
[8] IEC 61000-2-9:1996 Electromagnetic compatibility (EMC) – Part 2: Environment - Section 9: Description of HEMP environment - Radiated disturbance. Basic EMC publication.
[9] IEC 61000-4-25 Electromagnetic compatibility (EMC) – Part 4-25: Testing and measurement techniques – HEMP immunity test methods for equipment and systems.
[10] AECTP-500 Electromagnetic Environmental Effects Test and Verification.
[11] Achour Y., Starzyński J., Jośko A.: Nanosecond EMP simulator using a new high voltage pulse generator, Electrotechnical Review, R. 93, 0/2017, [doi] doi:10.15199/48.2017.10.07.
[12] Merla C., Amari S., Kenaan M., Liberti M., Apollonio F., Arnaud-Cormos D., Couderc V., Leveque P.: A 10-Ohm High-Voltage Nanosecond Pulse Generator, IEEE Transactions on Microwave Theory and Techniques, 2010, [doi] doi.org/10.1109/TMTT.2010.2086470.
[13] Lassalle F., Morell A., Loyen A., Chanconie T., Roques B., Toury M., Vezinet R.: Development and Test of a 400-kV PFN Marx With Compactness and Rise Time Optimization, IEEE Transactions on Plasma Science, 2018, [doi] doi.org/10.1109/TPS.2018.2837344.
[14] Zhang H., Shu T., Liu S., Zhang Z., Song L., Zhang H.: A Compact Modular 5 GW Pulse PFN-Marx Generator for Driving HPM Source, Electronics, 2021, [doi] doi.org/10.3390/electronics10050545.
[15] Kuffel E., Zaengl W. S., Kuffel J.: High Voltage Engineering Fundamentals, Elsevier Ltd., ISBN 978-0-7506-3634-6, 2000, [doi] doi.org/10.1016/b978-0-7506-3634-6.x5000-x.
[16] Starzyński J.: Symulacje komputerowe w projektowaniu kompaktowych generatorów szybkich impulsów pola elektromagnetycznego, OWPW, ISBN 978-83-7814-925-5, 2019.
[17] Chaber B., Łodyga W.: A Realistic Spark-Gap Model in Computer Simulation of Blumlein Transmission Line, Energies, 15, 11.2022, 2022, [doi] doi.org/10.3390/en15113919.
[18] Basso B.: Spice model simulates spark-gap arrestor, END Magazine, jul, pp. 3–5, 1997.
[19] Zych P., Sobolewski K., Sroka J., Roszczyk R., Kawamata K.: Comparative analysis of electric arc by simulation tests and practical measurements of a simple relay, 23rd International Conference on Computational Problems of Electrical Engineering (CPEE), pp. 1–4, 2022, [doi] 10.1109/CPEE56060.2022.9919675.
[20] Paschen F.: Über die zum Funkenübergang in Luft, Wasserstoff und Kohlensäure bei verschiedenen Drucken erforderliche Potentialdifferenz, Annalen der Physik, 273, 5, pp. 69–96, 1889, [doi] 10.1002/andp.18892730505.
[21] Rąbkowski J., Łasica A., Zdanowski M., Wrona G., Starzyński J.: Portable DC Supply Based on SiC Power Devices for High-Voltage Marx Generator, Electronics, 10, 313, 2021, [doi] 10.3390/electronics10030313.
[22] Montena – Field sensors. [web page] https://www.montena.com/. [Accessed on 4 May 2022.].
[23] Montena – Fibre-optic links. [web page] https://www.montena.com/. [Accessed on 4 May 2022.].